Published in final edited form as:
Cell. 2013 August 1; 154(3): 664–675. doi:10.1016/j.cell.2013.06.030.

Transformed *Drosophila* Cells Evade Diet-Mediated Insulin Resistance Through Wingless Signaling

Susumu Hirabayashi[1], **Thomas J. Baranski**[2], and **Ross L. Cagan**[1,3]

[1]Department of Developmental and Regenerative Biology, Annenberg 25-40, Icahn School of Medicine at Mount Sinai, One Gustave L. Levy Place, Box 1020, New York, NY 10029

[2]Department of Medicine, Washington University School of Medicine, 660 S. Euclid Ave., Box 8127, St. Louis, MO 63110

SUMMARY

Risk of specific cancers increases in patients with metabolic dysfunction including obesity and diabetes. Here we use *Drosophila* as a model to explore the effects of diet on tumor progression. Feeding *Drosophila* a diet high in carbohydrates was previously demonstrated to direct metabolic dysfunction including hyperglycemia, hyperinsulinemia and insulin-resistance. We demonstrate that high dietary sugar also converts Ras/Src transformed tissue from localized growths to aggressive tumors with emergent metastases. While most tissues displayed insulin resistance, Ras/Src tumors retained insulin pathway sensitivity, increased the ability to import glucose, and resisted apoptosis. High dietary sugar increased canonical Wingless/Wnt pathway activity, which upregulated Insulin Receptor gene expression to promote insulin sensitivity. The result is a feed-forward circuit that amplified diet-mediated malignant phenotypes within Ras/Src transformed tumors. By targeting multiple steps in this circuit with rationally applied drug combinations, we demonstrate the potential of combinatorial drug intervention to treat diet-enhanced malignant tumors.

INTRODUCTION

The prevalence of metabolism-related diseases including type 2 diabetes and obesity has been increasing worldwide. Metabolic disease impacts body homeostasis, leading to a constellation of symptoms including cardiovascular disease, blindness, neuropathy, and nephropathy. Recently, the American Diabetes Association and American Cancer Society jointly published a consensus report emphasizing accumulating evidence that patients with diabetes also show elevated risks of specific cancer types (Giovannucci et al., 2010). Epidemiological studies have provided strong evidence for the association between cancer and metabolic diseases including diabetes and obesity (Barone et al., 2008; Calle et al., 2003; Coughlin et al., 2004; Inoue et al., 2006): patients with metabolic dysfunction have both a higher incidence of specific tumors types and higher overall cancer-related mortality. For example, obese patients with progesterone receptor-negative breast cancer had a higher risk of lymph node metastasis, suggesting that metabolic dysfunction can promote tumor aggressiveness (Maehle et al., 2004). The increase in metabolic diseases worldwide

[3]For correspondence: Ross.Cagan@mssm.edu.

highlights metabolic dysfunction as an increasing issue in cancer progression. However, the mechanisms by which metabolic dysfunction contribute to cancer progression remain poorly understood.

Obesity and type 2 diabetes are typically associated with chronic hyperinsulinemia: levels of insulin in the blood rise to compensate for insulin resistance. Increased circulating insulin levels are in turn a risk factor for the development of hepatocellular carcinoma and colorectal cancer (Donadon et al., 2009; Kaaks et al., 2000). Together with the well-documented mitogenic effects of insulin (Ish-Shalom et al., 1997), this evidence suggests a role for hyperinsulinemia as a promoter of enhanced tumorigenesis in obese and diabetic patients. However, the development of insulin resistance in metabolism-related diseases raises a key question: how do tumors overcome insulin resistance to take advantage of increasing insulin levels? Here we utilize *Drosophila* to explore the effects of high dietary sugar on tumor progression *in vivo*.

Feeding *Drosophila* a diet supplemented to 1.0 M sucrose led to insulin resistance, hyperglycemia, increased insulin levels (hyperinsulinemia), and accumulation of fat, phenocopying important aspects of type 2 diabetes (Musselman et al., 2011). We used this model to explore the effects of high dietary sugar on tumor progression *in vivo*. On a normal diet, Csk/Src-dependent tumors were eliminated from the epithelium either alone or when paired with an oncogenic Ras isoform. In contrast, elevated dietary sugar strongly synergized with Ras/Src to generate large tumors associated with aggressive metastasis-like behavior. Using this model system, we investigated whether increased insulin levels underlie induction of malignant tumors. Importantly, Ras/Src-activated tumors remained sensitive to insulin in dietary conditions that promoted insulin resistance in surrounding tissues. We demonstrate that increased insulin/PI3K signaling in turn prevents apoptosis and promotes canonical Wingless/Wnt mitogenic signaling in Ras/Src tumors. Our results provide functional data that, in the face of high dietary sugar, Ras/Src-activated cells escape insulin resistance to exhibit enhanced growth that is dependent on Wingless/Wnt mitogenic signaling.

RESULTS

High dietary sucrose enhanced tumor growth

Feeding *Drosophila* a standard diet supplemented to 1.0 M sucrose (high dietary sucrose or “HDS”) led to metabolic defects reminiscent of specific aspects of type 2 diabetes including insulin resistance, hyperglycemia, elevated *Drosophila* Insulin-like peptide (DILP) levels, and accumulation of body fat (Musselman et al., 2011). To explore the link between metabolic dysfunction and tumor progression, we compared *Drosophila* cancer models fed HDS to those fed a control (0.15 M sucrose) diet. Combined elevation of Ras and Src pathway activities is a common motif in multiple cancer types including breast, colorectal, and pancreatic (Ishizawar and Parsons, 2004; Morton et al., 2010). Experimentally, oncogenic K-Ras plus Src isoforms cooperate to accelerate the onset of pancreatic ductal adenocarcinoma in mice models, and Ras plus Src act together to promote tumorigenesis in *Drosophila* (Shields et al., 2011; Vidal et al., 2007). We further developed this model by pairing transgenes that express oncogenic $ras1^{G12V}$ in the eye with the genotypically null $csk^{Q156Stop}$ allele of Csk, a primary negative regulator of Src kinase. Clones were labeled with GFP to visualize tumor progression. In control eyes, GFP expression was comparable in control diet *vs.* HDS, indicating that high sucrose feeding did not alter transgene expression levels (Figures 1A and 1B).

Genotypically *csk* null clones alone were rarely obtained when fed either control diet or HDS (Figures 1C and 1D) due to Src-mediated apoptosis (Vidal et al., 2006). Also as

previously reported (Pagliarini and Xu, 2003), targeting *ras1*^{G12V} to the eye resulted in isolated benign tumors that in turn led to lethality as pupae (Figure 1E). *ras1*^{G12V} animals fed HDS exhibited at most a mild increase in growth within the eye field (Figure 1F). Eyes with elevated Ras plus Src activity (*ras1*^{G12V}*;csk*$^{-/-}$) raised on a control diet displayed fewer and smaller GFP-positive clones compared to *ras1*^{G12V}-expressing clones alone (Figures 1E and 1G), indicating that *ras1*^{G12V} expression cannot overcome elimination of *csk* mutant cells.

By striking contrast, clones displayed strongly increased proliferation in 96.5% of *ras1*^{G12V}*;csk*$^{-/-}$ larvae fed HDS. The result was striking overgrowth and a significantly enlarged GFP-positive eye field that dominated the head region (Figures 1H and 1I). This overgrowth had consequences on animal viability: a majority (77.5%) of *ras1*^{G12V}*;csk*$^{-/-}$ animals fed HDS failed to initiate pupariation, instead dying as larvae with multiple secondary tumors (Figure S1A). Together, these results indicate that the metabolic status of the animals—as influenced by diet—strongly affects the outcome of Ras/Src-mediated tumorigenesis in the eye epithelium.

HDS feeding led to an approximately four day delay in completion of larval development (Musselman et al., 2011) (Figure S1B); therefore, phenotypes were compared between developmental stage matched animals fed HDS *vs.* control diet (late third instar larvae). To rule out the possibility that enhanced tumor growth in HDS fed animals was due to their older chronological age, we also analyzed progressive clone sizes in chronological age matched animals (Figures 1K–1S). At day 9 after egg laying (AEL), HDS fed larval eye tissue was significantly smaller than age-matched controls (12.9%; Figures 1M′, 1N′ and S1C) but the percentage area occupied by GFP-positive clones was already significantly larger: 13.5% in control diet, 42.8% in HDS (Figures 1M′, 1N′ and 1S). This difference widened over time: control clones decreased from 35.2% (day 7 AEL) to 13.5% (day 9 AEL) of total area while HDS clones progressively increased, reaching 58.9% at day 11 AEL and 93.7% at day 13 AEL (Figures 1K–1S). These analyses further support a role for HDS in enhancing growth of *ras1*^{G12V}*;csk*$^{-/-}$ tumors.

HDS but not high fat induced cancer phenotypes

Diets containing 2.0 M glucose enhanced *ras1*^{G12V}*;csk*$^{-/-}$ growth at a level similar to diets containing 1.0 M sucrose (Figure 1H and S2A). Other diets including pure banana that have similar carbohydrate content yielded similar tumor enhancement (Figure S2B), further emphasizing the specific role of high dietary carbohydrates. By contrast, *ras1*^{G12V}*;csk*$^{-/-}$ tumors failed to show enhanced tumor growth in a calorie-matched high fat diet (Figure S2C), indicating that high levels of dietary carbohydrates—but not high total caloric levels—are responsible for the enhanced cancer phenotype. This is consistent with observations that a high carbohydrate diet in general leads to metabolic defects in Drosophila not observed with calorie-matched high fat or high protein diets (Musselman et al., 2011).

HDS promoted aspects of invasive migration and distant secondary tumors

Basement membrane degradation by Matrix Metalloproteases (MMPs) is a key early step in the initiation of cell spreading and metastasis (Deryugina and Quigley, 2006). Eye epithelia from *ras1*^{G12V}*;csk*$^{-/-}$ animals fed a control diet displayed an intact basement membrane as assessed by Laminin A (Figure 2A). HDS feeding led to broad loss of Laminin A; loss was already evident at day 9 AEL (Figure 2B and S2D). However, *ras1*^{G12V}*;csk*$^{-/-}$-mediated up-regulation of MMP1 expression was independent of dietary sugar (Figures 2E and 2F). Our data suggests that HDS enhances breakdown of the basement membrane to facilitate spreading and metastasis-like behavior of transformed cells, at least in part by mechanisms independent of MMP1 expression levels.

Larvae fed HDS consistently (93.0%) displayed GFP-labeled *ras1*^{G12V};*csk*$^{-/-}$ cells scattered throughout their hemolymph, a blood analog (Figures 2I–2K and 2S). 19.1% of these larvae also developed secondary *ras*^{G12V};*csk*$^{-/-}$ tumors distant from the eye field that continued to proliferate (Figures 2L, 2P and 2S); secondary tumors were rarely (0.8%) observed in animals fed control food (Figure 2S). Whereas the percentage of animals with loss of Laminin in the eye tissue correlated with the percentage of animals with GFP-positive cells in the hemolymph, readily scorable secondary tumors were found in only a subset (19.1%) of the animals fed HDS (Figure 2S).

Combining *ras1*^{G12V} with a weaker *csk* allele, *csk*^{j1D8} (*ras1*^{G12V};*csk*$^{hypo/hypo}$) led to a reduced penetrance of secondary tumors (Figures S2E, S2F, S2F′ and S2G), suggesting that levels of Src activity play a primary role in distant Ras/Src tumor formation. We also examined *scribbled*, which encodes a protein required to maintain apical/basal cell polarity (Bilder and Perrimon, 2000). As previously reported (Pagliarini and Xu, 2003), targeting *ras1*^{G12V};*scrib*$^{-/-}$ to the eye led to substantial overgrowth; however, we did not observe secondary tumors in these animals when fed either a control diet or HDS (Figures S2H, S2I and S2J). These results indicate a specific relationship between Ras and Csk/Src activities that, when combined with HDS, synergize to produce secondary tumors. The data also indicate that tumor overgrowth and secondary tumor formation are separable processes and, similar to mammals (Mehlen and Puisieux, 2006), only a small subset of circulating cells successfully seed a secondary tumor.

Larger secondary *ras1*^{G12V};*csk*$^{-/-}$ tumors were typically tightly associated with the tracheal system, a tubular network that transports oxygen (Figures 2L–2O). A Chitin-binding probe (Devine et al., 2005) indicated that secondary tumors enwrapped tracheal branches (Figure 2Q). Interestingly, Chitin was abnormally deposited within these tumor-imbedded trachea (Figure 2Q), suggesting either tracheal alteration or *de novo* branching. Consistent but not proving the latter view, secondary *ras1*^{G12V};*csk*$^{-/-}$ tumors expressed Branchless (Figure 2R), a fly FGF ortholog capable of promoting *de novo* trachea branching (Sutherland et al., 1996). Together, these results indicate that HDS enhances or establishes multiple aspects of tumorigenesis in the presence of activated Ras/Src including proliferation, a block in apoptosis, invasive migration, and establishment of secondary tumors distant from the primary tumor.

The PI3K pathway mediates diet-induced tumorigenesis

Genetically reducing PI3K activity through a hypomorphic allele of *akt* (*ras1*^{G12V};*csk*$^{-/-}$,*akt*$^{hypo/hypo}$; Figure 3B) or through feeding of the PI3K inhibitor wortmannin (Figure S3) led to strongly reduced tumor cell survival in the presence of HDS. The Tor-class inhibitor rapamycin displayed a similar reduction in tumor tissue (Figure S3); in addition, animals were significantly smaller with an extended third instar larval stage as previously reported (Zhang et al., 2000). Conversely, co-expressing the constitutively active Insulin receptor isoform *inR*^{CA} (*inR*^{CA},*ras1*^{G12V};*csk*$^{-/-}$) in animals fed a control diet prevented elimination of clones from the epithelia. The result was tumor overgrowth in which 91.0% of larvae displayed an enlarged eye disc phenotype (Figures 3D and 3F). *inR*^{CA},*ras1*^{G12V};*csk*$^{-/-}$ animals did not exhibit any further increase in primary tumor size when raised on HDS (Figure 3E), nor did they exhibit enhanced tumors when compared to *ras1*^{G12V};*csk*$^{-/-}$ in HDS (compare Figure 1J and 3F). We conclude that components of the Insulin/PI3K pathway are required autonomously within the *ras1*^{G12V};*csk*$^{-/-}$-transformed cells for enhancement by HDS.

Of note, Insulin/PI3K signaling did not mediate all effects of HDS. While the triple combination *inR*^{CA},*ras1*^{G12V};*csk*$^{-/-}$ fed a control diet exhibited strongly enhanced expansion of tumors within the eye field, overgrowth was not accompanied by metastasis-

like behavior or secondary tumor formation. Further, though elevated MMP1 expression was observed the basement membrane was still retained (Figures 2C and 2G). This result again emphasizes that tumor overgrowth and metastasis are separable processes.

Ras/Src-activated cells remain sensitive to Insulin and glucose

Our results suggest that insulin signaling is required to mediate HDS-enhanced growth. However, eye epithelial tissue in control animals raised on HDS exhibited reduced phosphorylated, activated Akt upon Insulin stimulation, an indication of insulin resistance as previously reported (Figure 3G (Musselman et al., 2011). This led us to a central question in tumor metabolism studies: How does a diet that promotes insulin resistance also enhance tumors in an Insulin/PI3K-dependent manner?

In contrast to controls, eye tissue within $ras1^{G12V};csk^{-/-}$ animals fed HDS exhibited an increase in baseline Akt when compared to control diet-fed animals (Figure 3H), suggesting these tissues were in fact not insulin resistant. Consistent with this view, challenging eye tissue from HDS animals with exogenous Insulin led to a strong increase in phospho-Akt (Figure 3H). Insulin-stimulated increase in phospho-Akt was observed autonomously within the $ras1^{G12V};csk^{-/-}$ clones (Figure 3I). These data indicate that activating the Ras and Src pathways reversed HDS-induced insulin resistance, leading to hypersensitive responsiveness to Insulin. The result was increased sugar flux: in the presence or absence of exogenous Insulin, $ras1^{G12V};csk^{-/-}$ animals raised on HDS displayed a significant increase in glucose uptake to a level comparable to the triple combination $inR^{CA},ras1^{G12V};csk^{-/-}$ (Figures 3J–3N). Reducing *akt* activity ($ras1^{G12V};csk^{-/-},akt^{hypo/hypo}$) blocked glucose uptake (Figure 3O). We conclude that $ras1^{G12V};csk^{-/-}$ cells escape diet-induced insulin resistance to utilize both increased insulin responsiveness and insulin pathway-dependent glucose uptake. We next explored the mechanisms by which transformed cells evade insulin resistance.

Tumors exhibit aspects of an ‘undead’ phenotype

A central hallmark of mammalian cancer is the ability of transformed cells to evade apoptosis. In *Drosophila* developing eye and wing epithelia, keeping otherwise apoptotic cells alive (‘undead’) by blocking effector caspase activity leads to aberrant tissue overgrowth due to compensatory proliferation of surrounding cells, a process designed to maintain tissue size and integrity (reviewed in (Bergmann and Steller, 2010; Fan and Bergmann, 2008; Martin et al., 2009). We used an antibody that recognizes the cleaved, active isoform of human caspase-3, a validated readout for activity of the *Drosophila* initiator caspase Dronc (Fan and Bergmann, 2010). We observed broad Dronc activity in $ras1^{G12V};csk^{-/-}$ clones of animals raised on a control diet (Figure 4A and S4A). A significant proportion of these cells were undergoing apoptotic cell death as assessed by TUNEL staining (Figure 4D and S4A).

In the presence of HDS, $ras1^{G12V};csk^{-/-}$ clones also exhibited broad cytosolic Dronc activity (Figure 4B and S4A). However, these clones were almost completely negative for apoptotic cell death as assessed by TUNEL and DAPI analysis (Figure 4E and S4A; data not shown); a few cells outside of the clone region were TUNEL positive. Insulin pathway activation alone was sufficient to mimic this block: $inR^{CA},ras1^{G12V};csk^{-/-}$ animals fed a control diet retained Dronc caspase activity but, again, were resistant to apoptotic cell death as assessed by TUNEL (Figures 4C, 4F and S4A). One candidate to block apoptosis in transformed cells is the caspase inhibitor *Drosophila* Inhibitor of apoptosis protein 1 (Diap1), which inhibits caspases downstream of Dronc (Ditzel et al., 2008). *diap1* gene expression and Diap1 protein levels were strongly increased in the $ras1^{G12V};csk^{-/-}$ clones of animals raised in HDS compared to animals fed a control diet (Figures 4G–4I, S4B and S4C). The triple combination $inR^{CA},ras1^{G12V};csk^{-/-}$ was sufficient to elevate *diap1*

expression and Diap1 protein levels in animals fed a control diet, whereas reduced *akt* activity ($ras1^{G12V};csk^{-/-},akt^{hypo/hypo}$) failed to elevate Diap1 in HDS animals (Figures 4J, S4D and S4E). These results indicate that elevation of insulin pathway signaling through HDS leads to elevated Diap1 and a block in apoptotic cell death downstream of cleaved, activated Dronc. Interestingly, secondary tumors retained *diap1* expression but lost Dronc activity (Figure S4G and S4H).

Increased Wingless/Wnt-signaling mediates diet-induced tumorigenesis

Previous work in Drosophila compensatory proliferation found that 'undead' cells also elevate expression of the Wnt ortholog Wingless (Wg); this mitogenic signal in turn directs local hyperplasia (Perez-Garijo et al., 2009). In $ras1^{G12V};csk^{-/-}$ eye clones, we detected low levels of Wg protein within the clones in animal fed a control diet (Figure 4K). Notably, Wg protein levels were strongly upregulated in animals fed HDS (Figures 4L and 4M). Reducing *akt* activity ($ras1^{G12V};csk^{-/-},akt^{hypo/hypo}$) prevented this elevation (Figure S4F), while the triple combination $inR^{CA},ras1^{G12V};csk^{-/-}$ displayed increased Wg levels in animals fed a control diet (Figure 4N). Activation of InR alone was not sufficient to elevate Wg levels (Figure S5A). We conclude that combining elevated InR, Ras, and Src activities leads to elevated Wg expression in discrete tumors.

Elevation of Wg contributed to tumor progression. Reducing Wg activity ($ras1^{G12V};csk^{-/-},wg^{RNAi}$) in animals fed HDS led to strong suppression of tumor growth (Figure 5B). Expression of a dominant-negative isoform of the downstream pathway effector Tcf tcf^{DN} ($ras1^{G12V};csk^{-/-},tcf^{DN}$) also suppressed tumor growth (Figure 5C), indicating that canonical Wg signaling is required for high sucrose-induced enhancement of tumorigenesis. As a result, while only 22.5% of $ras1^{G12V};csk^{-/-}$ animals successfully initiated pupariation when fed HDS, 100% of $ras1^{G12V};csk^{-/-}wg,^{RNAi}$ or $ras1^{G12V};csk^{-/-},tcf^{DN}$ animals successfully pupariated when fed HDS (Figures S5B and S5C).

In 'undead' cells, Jnk pathway signaling is required for ectopic Wg expression (Ryoo et al., 2004). Expressing a dominant-negative isoform of the Drosophila Jnk ortholog Basket bsk^{DN} ($ras1^{G12V};csk^{-/-},bsk^{DN}$) suppressed tumor growth in HDS (Figures 5D and S5D) and blocked the elevation in Wg protein levels (Figure 5E), indicating that Wg upregulation is downstream of Bsk. Wg was also blocked in $inR^{CA},ras1^{G12V};csk^{-/-},bsk^{DN}$ eye clones of animals fed a control diet, indicating Bsk is in turn downstream of InR with regard to elevated Wg (Figure 5F). Together, these results indicate that $ras1^{G12V};csk^{-/-}$ cells achieve an 'undead' status through Diap1, which then activates a InR-Jnk-Wg pathway that promotes cell autonomous proliferation. We next asked whether this ability of Wg to mediate key aspects of HDS/insulin pathway activity within Ras/Src-activated tumors extended to evasion of insulin resistance.

Canonical Wingless/Wnt pathway signaling promotes Insulin sensitivity by regulating InR expression

In organ culture experiments from animals fed HDS, challenging control tissue with exogenous Insulin led to little or no increase in pathway activity as assessed by phosphorylated Akt (Figure 5G); we also observed significant downregulation of *inR* mRNA (Figure 5H), which presumably at least partially accounts for the tissues' insulin resistance. Two other members of the Insulin pathway, Chico/IRS and Lnk/SH2B, showed no change in transcript levels (Figure 5H), suggesting that diet-directed downregulation is specific to InR. In contrast, tissue expressing Wg responded to exogenous Insulin by strongly activating pathway signaling (Figure 5G). This suggests that—in addition to Insulin

regulating Wg—Wg regulates Insulin signaling, potentially through regulation of *inR* expression.

Consistent with this model, *inR* mRNA levels were significantly upregulated in $ras1^{G12V};csk^{-/-}$ eye clones in animals fed HDS (Figure 5I). The result was an increase in phosphorylated, activated InR that was strongly enhanced when the tissue was challenged with exogenous Insulin (Figure 5J). Importantly, the diet-dependent increase in *inR* mRNA levels was suppressed by reducing activity of the Wg target Tcf ($ras1^{G12V};csk^{-/-},tcf^{DN}$; Figure 5I). These results indicate that canonical Wg signaling promotes insulin sensitivity by upregulating *inR* transcripts. That is, transformed tissue evaded insulin resistance through a feed forward mechanism by which elevated Wg directs elevated InR (Figure 5K).

Combinatorial multi-node drug treatments for diet-induced Ras/Src-tumorigenesis

Identifying an HDS-dependent 'undead' cell phenotype in $ras1^{G12V};csk^{-/-}$ tissue suggested specific points of therapeutic intervention: (i) conversion of dietary sucrose, (ii) InR/PI3K metabolic signaling, (iii) canonical Wg/Wnt pathway 'undead' cell signaling, and (iv) Ras plus Src oncogenic pathways(Fig. 5K). Nearly three-quarters of $ras1^{G12V};csk^{-/-}$ animals raised on HDS failed to pupariate due to aggressive eye tumors; we utilized pupariation rate as a quantitative viability assay to take a stepwise approach towards identifying an optimized whole animal therapeutic cocktail. Time to pupariation was not affected by drug treatments when compared to vehicle (DMSO) treatment alone; pupariation rates were assessed at day 17 AEL, after pupariation curves reached a plateau (Figure S6A).

Acarbose is an inhibitor of alpha-glucosidase that is used to treat type 2 diabetes mellitus (Anderson, 2005). Feeding acarbose in the presence of HDS led to reduced tumor growth and improved $ras1^{G12V};csk^{-/-}$ animal survival (Figures 6B and 6J). Pyrvinium, a small-molecule inhibitor of canonical Wnt-signaling pathway (Thorne et al., 2010), suppressed HDS-induced tumor growth at a concentration that did not affect growth of wild type clones (Figures 6C and S6B): 41.9% of HDS- and pyrvinium-fed animals achieved pupariation (Figure 6J). We recently developed polypharmacological anti-cancer compounds (Dar et al., 2012) that target the Ras, Src, and Tor pathways as single agents. These represent the central cellular pathways that mediate HDS-induced tumor growth in $ras1^{G12V};csk^{-/-}$ animals and, indeed, the compound AD81 suppressed Ras/Src-tumorigenesis and larval lethality of animals fed HDS (Figures 6D and 6J). Biochemical analysis of dissected eye tissues supported inhibition of Ras, Src and Tor pathways by AD81 feeding, though not by the close analog AD80 (Figure 6I; (Dar et al., 2012). Furthermore, AD81 also suppressed tumor growth and larval lethality of $inR^{CA},ras1^{G12V};csk^{-/-}$ animals fed a control diet, demonstrating AD81 can act tumor-autonomously (Figure S6C).

Targeting sugar or the Ras, Src, Pi3K, or Wg pathways showed significant but limited efficacy on $ras1^{G12V};csk^{-/-}$ tumors in animals fed HDS. Combining acarbose with pyrvinium, acarbose with AD81, or pyrvinium with AD81 enhanced survival to permit 64.4%, 62.9%, and 68.5%, survival of $ras1^{G12V};csk^{-/-}$ animals to pupariation in the presence of HDS, respectively (Figures 6E–6G, and 6J). Strikingly, the triple combination acarbose-pyrvinium-AD81 achieved a 91.2% rescue level of $ras1^{G12V};csk^{-/-}$ animals fed HDS (Figures 6H and 6J), far higher than any single or double drug combination we have tested. We conclude that targeting multiple nodes in a rational manner may be required to achieve an optimal therapeutic index, balancing efficacy with minimal whole animal toxicity.

DISCUSSION

Epidemiological studies provide strong evidence for an association between metabolism-related diseases and cancer but the underlying mechanisms that link these two diseases remain poorly understood. In this study, we demonstrate that dietary sucrose strongly enhances multiple aspects of Ras/Src-activated tumors in *Drosophila*. HDS led to stabilization of tumors within the epithelium, increased proliferation, and metastasis-like behavior. Mechanistically, we provide evidence that Ras/Src-activated cells increase insulin pathway-sensitivity in an otherwise insulin-resistant environment, allowing them to take advantage of high circulating glucose. The result is a Wg- and Jnk- dependent enhancement of tumor progression. Our results support a model in which Ras/Src cells become hypersensitive to circulating insulin, leading to efficient activation of insulin/PI3K signaling (Figure 5K).

A key consequence of increased insulin/PI3K signaling was prevention of apoptosis and promotion of elevated levels of Wg expression and activity; these two aspects promoted an 'undead'-like cell phenotype that further enhanced proliferation. We observed low but detectable levels of Wg expression in $ras1^{G12V};csk^{-/-}$ clones in animals fed a control diet (Figure 4K); these clones exhibited high levels of apoptosis. In contrast, Wg accumulated at significantly higher levels in $ras1^{G12V};csk^{-/-}$ tumors within animals fed HDS (Figure 4L). High Wg levels led to elevated Diap1 expression and reduced apoptosis, stabilizing $ras1^{G12V};csk^{-/-}$ clones and revealing accumulation of Wg within the clone. Our model suggests that inhibition of cell death in 'HDS tumors' is a key aspect of Ras/Src-mediated transformation may allow cells to stably and continuously produce Wg. Wg was expressed within $ras1^{G12V};csk^{-/-}$ cells in the presence of HDS (Figure 4L and 4M) and phosphorylated Akt levels increased within Ras/Src clones but not detectably in nearby wild type cells (Figure 3I). Therefore, unlike the conventional undead situation—induced by Hid plus P35—a Wg mediated increase in InR expression and signaling provides a growth advantage specifically within Ras/Src cells rather than surrounding wild type tissue. Together, our data provide evidence that the 'undead' cell phenotype generates an InR-Jnk-Wg-InR feed-forward mechanism that results in elevated InR expression and a reversal of insulin resistance (Figure 5K). The result is transformed tissue that is optimized for insulin-dependent glucose uptake in an animal with hyperinsulinemia and hyperglycemia.

The 'undead' phenotype was not fully maintained in secondary tumors: Dronc expression was lost in distant tumors of $ras1^{G12V};csk^{-/-}$, though *diap1* expression was maintained (Figure S4G and S4H). These results suggest that secondary tumors develop progressively distinct properties; understanding these changes will require additional studies. A Chitin-binding probe suggested progressive steps of tubule maturation within secondary tumor-associated trachea including potentially newly expressed Chitin scattered within immature tubules, tubules filled with solid projections of Chitin, and hollowed out mature tubules (Figure 2Q). Additional studies will be required to confirm that this represents neo-tracheogenesis and, if so, whether this occurs through processes reminiscent of the neo-angiogenesis that is a common feature of mammalian metastasis (Bergers and Benjamin, 2003). Strikingly, secondary tumors expressed high levels of the FGF ortholog Branchless, an important step in promoting tracheogenesis during development (Figure 2R; (Sutherland et al., 1996)).

The Drosophila Wnt ortholog Wg promotes tumors' ability to evade insulin-resistance through its regulation of *inR* expression in the presence of HDS feeding, which otherwise promotes diabetes-like phenotypes (Figure 5H; (Musselman et al., 2011). High Wg expression requires both Ras/Src-activation and HDS, promoting *inR* expression through canonical Wg-dTcf signaling (Figure 5I). These results emphasize a link between canonical

Wg signaling and Insulin-signaling. Consistent with this model linking canonical Wg and Insulin signaling pathways, a recent study reports that reduced expression of skeletal muscle Insulin Receptor—linked to hyperinsulinemia and insulin resistance—is enhanced by a mutation in the Wnt co-receptor LRP6 in humans (Singh et al., 2013)

Tumors with Wnt-activation may represent tumor types that respond and synergize with metabolic defects. Wnt-activation is frequently observed in many tumor types including those with strong association with diabetes such as hepatocellular carcinomas and colorectal cancers; activating mutations in β-catenin and loss of function mutation in APC is frequently found in human hepatocellular carcinoma and colorectal cancers (Fodde et al., 2001; Laurent-Puig and Zucman-Rossi, 2006). Incidence of pancreatic cancer has a particularly strong association with diabetes, suggesting its constituent mutation load may interface with metabolic dysfunction. Activating mutations in K-Ras plus up-regulation of Src activity are commonly found in pancreatic ductal adenocarcinoma (PDA) (Almoguera et al., 1988; Morton et al., 2010), and a mouse K-Ras/Src pancreatic model developed PDA with shortened latency (Shields et al., 2011). Wnt ligands and transcriptional target genes of β-catenin are highly expressed in PDA (Pasca di Magliano et al., 2007), a phenomenon reminiscent of our observations linking diet, Ras/Src, and Wnt signaling. A clear link has yet to be established between pancreatic cancers featuring elevated Ras/Src activity and/or Wnt-pathway activation within diabetic patients.

Our data indicate that limiting dietary sucrose directly or through blocking its intermediates through compounds such as Acarbose may reduce important aspects of tumor risk and progression in individuals with metabolism-related diseases. Combining acarbose with drugs that target the triggering Ras/Src pathways plus components of the amplification circuit provided the most robust therapeutic impact on diet-enhanced tumors in our model. These results provide a potential explanation for how insulin resistant animals are at increased risk for tumorigenesis, and emphasize the importance of targeting multiple, specific nodes to achieve optimal therapeutic value.

EXPERIMENTAL PROCEDURES

Fly Stocks

UAS-ras1^{G12V}, UAS-inR^{A1325D} (inR^{CA}), akt^{04226}, csk^{j1D8}, UAS-tcf^{DN}, UAS-bsk^{DN}, UAS-HA-wg flies were obtained from the Bloomington *Drosophila* Stock Center. *UAS-wg^{RNAi}* flies were obtained from Vienna *Drosophila* RNAi Center. The following stocks were kindly provided to us: *FRT82B, csk^{Q156Stop}* by A. O'Reilly and M. Simon; *scrib^{1}* by D. Bilder; *ey(3.5)-FLP1* by G. Halder.

To create eyeless-driven green fluorescent protein (GFP)–labeled clones, flies with the genotype *ey(3.5)-FLP1; act>y+>gal4, UAS-GFP; FRT82B, tub-gal80* were crossed with flies with the following genotypes: (a) *UAS-lacZ; FRT82B*; (b) *UAS-lacZ; FRT82B, csk^{Q156Stop}/TM6b*; (c) *UAS-ras1^{G12V}; FRT82B*; (d) *UAS-ras1^{G12V}; FRT82B, csk^{Q156Stop}/TM6b*; (e) *UAS-ras1^{G12V}; FRT82B, csk^{j1D8}/TM6b*; (f) *UAS-ras1^{G12V}; FRT82B, scrib^{1}/TM6b*; (g) *UAS-inR^{A1325D}, UAS-ras1^{G12V}; FRT82B, csk^{Q156Stop}/TM6b*; (h) *UAS-ras1^{G12V}; FRT82B, csk^{Q156Stop}, akt^{04226}/TM6b*; (i) *UAS-ras1^{G12V}; FRT82B, csk^{Q156Stop}, UAS-wg^{RNAi}/TM6b*; (j) *UAS-ras1^{G12V}; FRT82B, csk^{Q156Stop}, UAS-tcf^{DN}/TM6b*; (k) *UAS-ras1^{G12V}; FRT82B, csk^{Q156Stop}, UAS-bsk^{DN}/TM6b. (l) UAS-inR^{A1325D}, UAS-ras1^{G12V}; FRT82B, csk^{Q156Stop}, UAS-bsk^{DN}/TM6b. (m) UAS-inR^{A1325D}; FRT82B. (n) FRT82B, UAS-HA-wg.*

Cultures

Cultures were carried out on Bloomington semi-defined medium (described by the Bloomington *Drosophila* stock center) with modifications. Detailed recipes for control diet, HDS, and high fat diet is previously described (Musselman et al., 2011). The following final concentrations of carbohydrates were included; 0.15 M sucrose (control diet), 1.0 M sucrose (HDS), 2.0 M glucose (high glucose diet). Cultures were performed at 25°C unless otherwise noted.

Immunofluorescenceand TUNEL Labeling

Larval eyes were dissected in PBS, fixed in 4% paraformaldehyde (PFA) in PBS or PLP-fixative (2.5% paraformaldehyde, 0.075 M lysine. 0.25% (w/v) Na-periodate in phosphate buffer), washed in PBT (PBS containing 0.1% Triton X-100), and incubated with primary antibodies in PAXDG (PBS containing 1% BSA, 0.3% Triton X-100, 0.3% deoxycholate, and 5% goat serum), followed by washing and incubation with secondary antibodies in PAXDG. Tissues were counter-stained with TO-PRO-3 (Invitrogen) and mounted in Vectashield mounting media (Vector Laboratories). Antibodies used were: rabbit anti-Cleaved Caspase-3 (Asp175; Cell Signaling), mouse anti-dMMP1 (DSHB: Developmental Studies Hybridoma Bank), mouse anti-Wingless (DSHB), mouse anti-beta-galactosidase (DSHB), rabbit anti-Laminin beta 1 (Abcam), rabbit anti-phospho-Histone H3 (Ser10; Millipore), rabbit anti-Diap1 (gift from H. Steller), rabbit anti-phospho-Akt (Ser473; Cell Signaling), rat anti-Branchless (gift from M. Krasnow). Secondary Alexa 568-conjugated anti-mouse and anti-rabbit antibodies were used (Molecular Probes). To label tracheal lumen, Rhodamine-conjugated Chitin-binding Probe was used (New England BioLabs).

TUNEL (terminal deoxynucleotidyl transferase–mediated deoxyuridine-triphosphate nick end-labeling) was performed using the TMR-Red In Situ Cell Detection Kit (Roche Diagnostics). Samples were fixed for 15 minutes in 4% PFA in PBT, washed in PBT and permeabilized in 100 mM sodium citrate/0.1% TritonX-100 at 65°C for 30 minutes, washed in PBT, and free DNA ends were fluorescein-labeled.

Fluorescent and confocal images were taken with Leica DM5500 microscope equipped with DFC340 FX Monochrome Digital Camera and TSC SPE confocal microscope.

Drugs

Compounds solubilized in DMSO were diluted directly into the fly medium and vortexed extensively to obtain homogeneous culture. Drugs used were: wortmannin and rapamycin (LC Laboratories); acarbose and pyrvinium pamoate (Sigma). AD compounds were provided by A. Dar and K. Shokat (UCSF).

Western Blotting

Wandering third instar larvae were rinsed in PBS, the eye-discs were dissected out, and placed in Schneider's *Drosophila* Medium on ice. The eye-discs were incubated with or without 5 μM recombinant human Insulin (Sigma) for 15 minutes at room temperature. Eye discs were transferred to a micro centrifuge tube, spun down briefly. The supernatant were discarded and the remaining precipitates were suspended in SDS sample buffer at a concentration of 10 μl/mg tissue and used to generate Western blots. Antibodies used targeted: total Akt (Cell Signaling), phospho-*Drosophila* Akt (Ser505; Cell Signaling), phospho-IGF-1 Receptor β (Tyr1131)/Insulin Receptor β (Tyr1146; Cell Signaling), and Syntaxin (DSHB). Secondary antibodies were from Cell Signaling.

Glucose Uptake Assay

For the glucose uptake experiments, flies with the genotype *ey(3.5) FLP1; act>y+>gal4; FRT82B, tub-gal80* were crossed with flies with the following genotypes: (a) *UAS-lacZ; FRT82B*; (b) *UAS-ras1^{G12V}; FRT82B, csk^{Q156Stop}/TM6b*; (c) *UAS-inR^{A1325D}, UAS-ras1^{G12V}; FRT82B, csk^{Q156Stop}/TM6b*; (d) *UAS-ras1^{G12V}; FRT82B, csk^{Q156Stop}, akt^{f4226}/TM6b*.

Wandering third instar larvae were rinsed in PBS, the eye-discs were dissected out, and placed in *Drosophila* Larval Saline (Hepes-NaOH (pH7.1), 87 mM NaCl, 40 mM KCl, 8 mM $CaCl_2$, 8 mM $MgCl_2$, 50 mM Sucrose, 5 mM Trehalose) on ice. The eye-discs were incubated with or without 5 μM recombinant human Insulin (Sigma) in the presence of 2-(*N*-(7-nitrobenz-2-oxa-1,3-diazol-4-yl)amino)-2-deoxyglucose (2-NBDG: Invitrogen) for 15 minutes at room temperature. The tissues were washed with *Drosophila* Larval Saline and mounted with a Vectashield (Vector Laboratories).

Quantitative RT-PCR

Total RNA was extracted from the eye discs using QIAGEN RNeasy Mini Kit. Oligo-dT primers and Superscript RT-II reverse transcriptase (Invitrogen) was used to synthesize first strand DNA. PCR was performed using Power SYBR Green PCR Master Mix (Applied Biosystems) and analyzed on Applied Biosystems StepOnePlus real-time PCR system. Results were normalized to *Kinesin* mRNA, and *RpL32* was used as a control. The following primers were used: Kinesin-f, 5′-GCTGGACTTCGGTCGTAGAG-3′; Kinesin-r, 5′-CTTTTCATAGCGTCGCTTCC-3′; RpL32-f, 5′-GCTAAGCTGTCGCACAAATG-3′; RpL32-r, 5′-GTTCGATCCGTAACCGATGT-3′; InR-f, 5′-ACAAAATGTAAAACCTTGCAAATCC-3′; InR-r, 5′-GCAGGAAGCCCTCGATGA-3′; chico-f, 5′-ATCAGGCGATGCGGTC-3′; chico-r, 5′-ACATAGCGCTCAGTATCG-3′; dLnk-f, 5′-GTGTTCGCCTAAAGACAAATGAAAT-3′; dLnk-r, 5′-TGTTAGCGTTGTGGGATCCAA-3′.

Supplementary Material

Refer to Web version on PubMed Central for supplementary material.

Acknowledgments

We thank J. Long, J. Na, J. Pendse, L. Palanker Musselman, M. Vidal and current and former Baranski and Cagan lab members for helpful discussions; CY. Nien for writing MATLAB scripts for quantitation; Y. Tomer and D. LeRoith for manuscript comments; and A. O'Reilly, M. Simon, D. Bilder, G. Halder, H. Steller, M. Krasnow, A. Dar and K. Shokat for the reagents. We also thank the Bloomington *Drosophila* Stock Center, Vienna *Drosophila* RNAi Center and Developmental Studies Hybridoma Bank for fly strains and antibodies. This research was supported by grants from the National Cancer Institute (R01CA170495, R01-CA109730; S. H., R. L. C.) and R21 DK069940 (R.L.C., T.J.B.). R.L.C. and T.J.B. are co-founders of Medros, Inc., which uses models of human disease for drug development.

References

Almoguera C, Shibata D, Forrester K, Martin J, Arnheim N, Perucho M. Most human carcinomas of the exocrine pancreas contain mutant c-K-ras genes. Cell. 1988; 53:549–554. [PubMed: 2453289]

Anderson DC Jr. Pharmacologic prevention or delay of type 2 diabetes mellitus. Ann Pharmacother. 2005; 39:102–109. [PubMed: 15562143]

Barone BB, Yeh HC, Snyder CF, Peairs KS, Stein KB, Derr RL, Wolff AC, Brancati FL. Long-term all-cause mortality in cancer patients with preexisting diabetes mellitus: a systematic review and meta-analysis. JAMA. 2008; 300:2754–2764. [PubMed: 19088353]

Bergers G, Benjamin LE. Tumorigenesis and the angiogenic switch. Nat Rev Cancer. 2003; 3:401–410. [PubMed: 12778130]

Bergmann A, Steller H. Apoptosis, stem cells, and tissue regeneration. Sci Signal. 2010; 3:re8. [PubMed: 20978240]

Bilder D, Perrimon N. Localization of apical epithelial determinants by the basolateral PDZ protein Scribble. Nature. 2000; 403:676–680. [PubMed: 10688207]

Calle EE, Rodriguez C, Walker-Thurmond K, Thun MJ. Overweight, obesity, and mortality from cancer in a prospectively studied cohort of U.S. adults. N Engl J Med. 2003; 348:1625–1638. [PubMed: 12711737]

Coughlin SS, Calle EE, Teras LR, Petrelli J, Thun MJ. Diabetes mellitus as a predictor of cancer mortality in a large cohort of US adults. Am J Epidemiol. 2004; 159:1160–1167. [PubMed: 15191933]

Dar AC, Das TK, Shokat KM, Cagan RL. Chemical genetic discovery of targets and anti-targets for cancer polypharmacology. Nature. 2012; 486:80–84. [PubMed: 22678283]

Deryugina EI, Quigley JP. Matrix metalloproteinases and tumor metastasis. Cancer Metastasis Rev. 2006; 25:9–34. [PubMed: 16680569]

Devine WP, Lubarsky B, Shaw K, Luschnig S, Messina L, Krasnow MA. Requirement for chitin biosynthesis in epithelial tube morphogenesis. Proc Natl Acad Sci U S A. 2005; 102:17014–17019. [PubMed: 16287975]

Ditzel M, Broemer M, Tenev T, Bolduc C, Lee TV, Rigbolt KT, Elliott R, Zvelebil M, Blagoev B, Bergmann A, et al. Inactivation of effector caspases through nondegradative polyubiquitylation. Mol Cell. 2008; 32:540–553. [PubMed: 19026784]

Donadon V, Balbi M, Zanette G. Hyperinsulinemia and risk for hepatocellular carcinoma in patients with chronic liver diseases and Type 2 diabetes mellitus. Expert Rev Gastroenterol Hepatol. 2009; 3:465–467. [PubMed: 19817667]

Fan Y, Bergmann A. Apoptosis-induced compensatory proliferation. The Cell is dead. Long live the Cell! Trends Cell Biol. 2008; 18:467–473. [PubMed: 18774295]

Fan Y, Bergmann A. The cleaved-Caspase-3 antibody is a marker of Caspase-9-like DRONC activity in Drosophila. Cell Death Differ. 2010; 17:534–539. [PubMed: 19960024]

Fodde R, Smits R, Clevers H. APC, signal transduction and genetic instability in colorectal cancer. Nat Rev Cancer. 2001; 1:55–67. [PubMed: 11900252]

Giovannucci E, Harlan DM, Archer MC, Bergenstal RM, Gapstur SM, Habel LA, Pollak M, Regensteiner JG, Yee D. Diabetes and cancer: a consensus report. CA Cancer J Clin. 2010; 60:207–221. [PubMed: 20554718]

Inoue M, Iwasaki M, Otani T, Sasazuki S, Noda M, Tsugane S. Diabetes mellitus and the risk of cancer: results from a large-scale population-based cohort study in Japan. Arch Intern Med. 2006; 166:1871–1877. [PubMed: 17000944]

Ish-Shalom D, Christoffersen CT, Vorwerk P, Sacerdoti-Sierra N, Shymko RM, Naor D, De Meyts P. Mitogenic properties of insulin and insulin analogues mediated by the insulin receptor. Diabetologia. 1997; 40(Suppl 2):S25–31. [PubMed: 9248698]

Ishizawar R, Parsons SJ. c-Src and cooperating partners in human cancer. Cancer Cell. 2004; 6:209–214. [PubMed: 15380511]

Kaaks R, Toniolo P, Akhmedkhanov A, Lukanova A, Biessy C, Dechaud H, Rinaldi S, Zeleniuch-Jacquotte A, Shore RE, Riboli E. Serum C-peptide, insulin-like growth factor (IGF)-I, IGF-binding proteins, and colorectal cancer risk in women. J Natl Cancer Inst. 2000; 92:1592–1600. [PubMed: 11018095]

Laurent-Puig P, Zucman-Rossi J. Genetics of hepatocellular tumors. Oncogene. 2006; 25:3778–3786. [PubMed: 16799619]

Maehle BO, Tretli S, Thorsen T. The associations of obesity, lymph node status and prognosis in breast cancer patients: dependence on estrogen and progesterone receptor status. APMIS. 2004; 112:349–357. [PubMed: 15511272]

Martin FA, Perez-Garijo A, Morata G. Apoptosis in Drosophila: compensatory proliferation and undead cells. Int J Dev Biol. 2009; 53:1341–1347. [PubMed: 19247932]

Mehlen P, Puisieux A. Metastasis: a question of life or death. Nat Rev Cancer. 2006; 6:449–458. [PubMed: 16723991]

Morton JP, Karim SA, Graham K, Timpson P, Jamieson N, Athineos D, Doyle B, McKay C, Heung MY, Oien KA, et al. Dasatinib inhibits the development of metastases in a mouse model of pancreatic ductal adenocarcinoma. Gastroenterology. 2010; 139:292–303. [PubMed: 20303350]

Musselman LP, Fink JL, Narzinski K, Ramachandran PV, Hathiramani SS, Cagan RL, Baranski TJ. A high-sugar diet produces obesity and insulin resistance in wild-type Drosophila. Dis Model Mech. 2011

Pagliarini RA, Xu T. A genetic screen in Drosophila for metastatic behavior. Science. 2003; 302:1227–1231. [PubMed: 14551319]

Pasca di Magliano M, Biankin AV, Heiser PW, Cano DA, Gutierrez PJ, Deramaudt T, Segara D, Dawson AC, Kench JG, Henshall SM, et al. Common activation of canonical Wnt signaling in pancreatic adenocarcinoma. PLoS One. 2007; 2:e1155. [PubMed: 17982507]

Perez-Garijo A, Shlevkov E, Morata G. The role of Dpp and Wg in compensatory proliferation and in the formation of hyperplastic overgrowths caused by apoptotic cells in the Drosophila wing disc. Development. 2009; 136:1169–1177. [PubMed: 19244279]

Ryoo HD, Gorenc T, Steller H. Apoptotic cells can induce compensatory cell proliferation through the JNK and the Wingless signaling pathways. Dev Cell. 2004; 7:491–501. [PubMed: 15469838]

Shields DJ, Murphy EA, Desgrosellier JS, Mielgo A, Lau SK, Barnes LA, Lesperance J, Huang M, Schmedt C, Tarin D, et al. Oncogenic Ras/Src cooperativity in pancreatic neoplasia. Oncogene. 2011; 30:2123–2134. [PubMed: 21242978]

Singh R, De Aguiar RB, Naik S, Mani S, Ostadsharif K, Wencker D, Sotoudeh M, Malekzadeh R, Sherwin RS, Mani A. LRP6 enhances glucose metabolism by promoting TCF7L2-dependent insulin receptor expression and IGF receptor stabilization in humans. Cell Metab. 2013; 17:197–209. [PubMed: 23395167]

Sutherland D, Samakovlis C, Krasnow MA. branchless encodes a Drosophila FGF homolog that controls tracheal cell migration and the pattern of branching. Cell. 1996; 87:1091–1101. [PubMed: 8978613]

Thorne CA, Hanson AJ, Schneider J, Tahinci E, Orton D, Cselenyi CS, Jernigan KK, Meyers KC, Hang BI, Waterson AG, et al. Small-molecule inhibition of Wnt signaling through activation of casein kinase 1alpha. Nat Chem Biol. 2010; 6:829–836. [PubMed: 20890287]

Vidal M, Larson DE, Cagan RL. Csk-deficient boundary cells are eliminated from normal Drosophila epithelia by exclusion, migration, and apoptosis. Dev Cell. 2006; 10:33–44. [PubMed: 16399076]

Vidal M, Warner S, Read R, Cagan RL. Differing Src signaling levels have distinct outcomes in Drosophila. Cancer Res. 2007; 67:10278–10285. [PubMed: 17974969]

Zhang H, Stallock JP, Ng JC, Reinhard C, Neufeld TP. Regulation of cellular growth by the Drosophila target of rapamycin dTOR. Genes Dev. 2000; 14:2712–2724. [PubMed: 11069888]

HIGHLIGHTS

- High dietary sugar enhances Ras/Src-mediated transformation in Drosophila
- Ras/Src-activated tumors evade diet-mediated insulin resistance
- Insulin resistance evasion is due to Wingless-mediated Insulin Receptor upregulation
- Rational targeting of multiple pathways can reduce diet-enhanced tumors

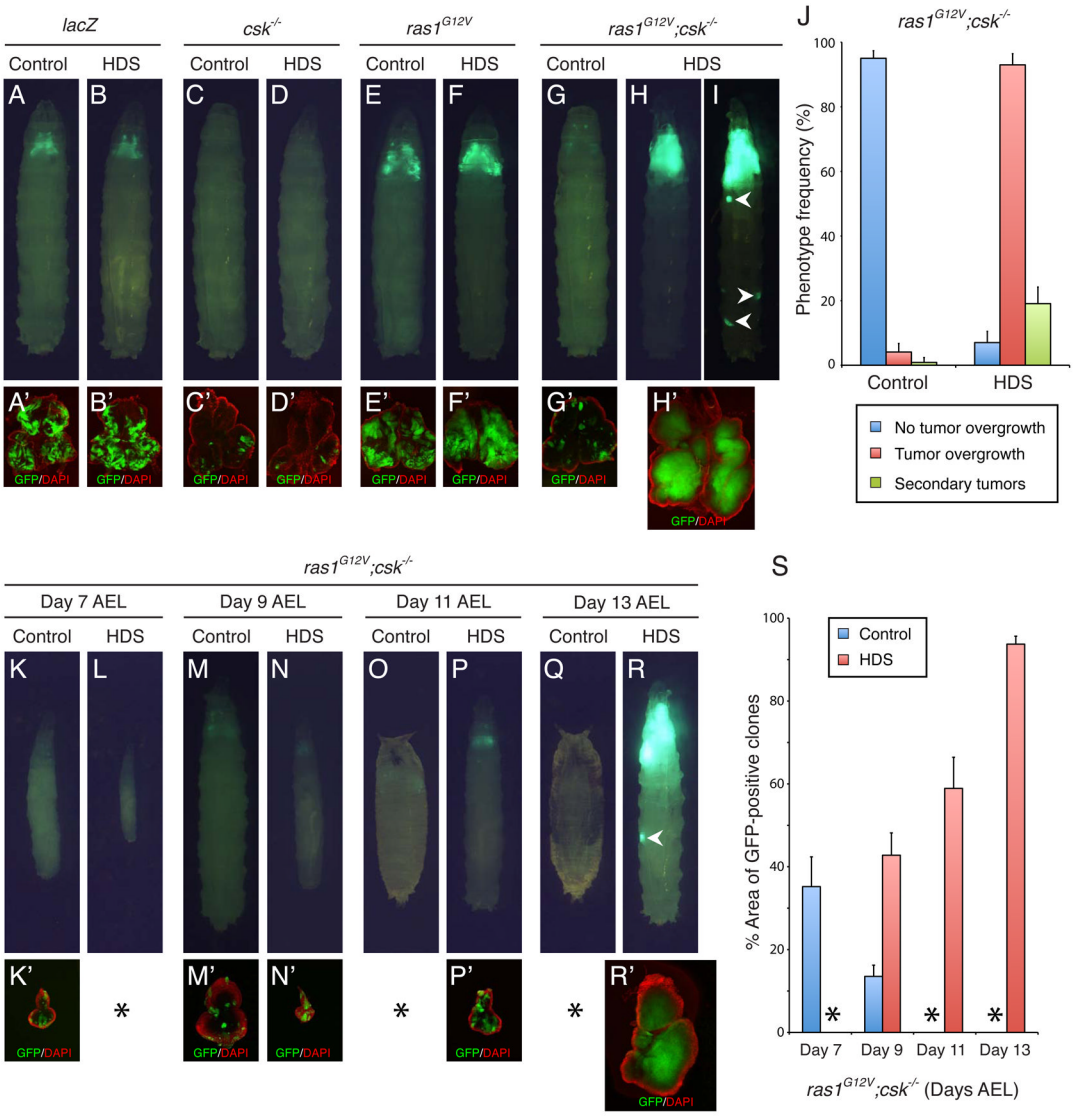

Figure 1. HDS diverts Ras/Src-activated cells into aggressive tumors

(A–I) Developmental stage matched third instar larvae fed control diet or HDS. (A and B) *lacZ* control in control diet (day 7 AEL) and HDS (day 11 AEL) (C and D) $csk^{-/-}$ in control diet (day 7 AEL) and HDS (day 11 AEL), (E and F) $ras1^{G12V}$ in control diet (day 8 AEL) and HDS (day 12 AEL), (G, H and I) $ras1^{G12V};csk^{-/-}$ in control diet (day 9 AEL) and HDS (day 13 AEL). The latter demonstrated secondary tumors in a subset of animals (arrowhead in I). (A′–H′), Matching dissected eye epithelial tissue stained with DAPI (red). (J) Quantitation of the observed phenotypes. Blue bar: eye discs without overgrowth (*e.g.;* Fig. 1G). Red bar: eye discs with tumor overgrowth and overall enlarged tissue size (*e.g.;* Fig. 1H). Green bar: animals with secondary tumors (*e.g.;* Fig. 1I). Results are shown as mean ± SEM. (K–R) Chronological age matched larvae fed control diet or HDS. $ras1^{G12V};csk^{-/-}$ animals shown at day 7 AEL (K and L), day 9 AEL (M and N), day 11 AEL (O and P), and day 13 AEL (Q and R). (K′, M′, N′, P′ and R′), Matching dissected eye epithelial tissue stained with DAPI (red). (S) Quantitation of the percentage of GFP-positive clone area percentage relative to total eye tissue area. Results are shown as mean ± SEM of individual eye discs. * Not assessed due to early (small discs, Day 7) or late (everted pupal discs) stages. See also Figure S1.

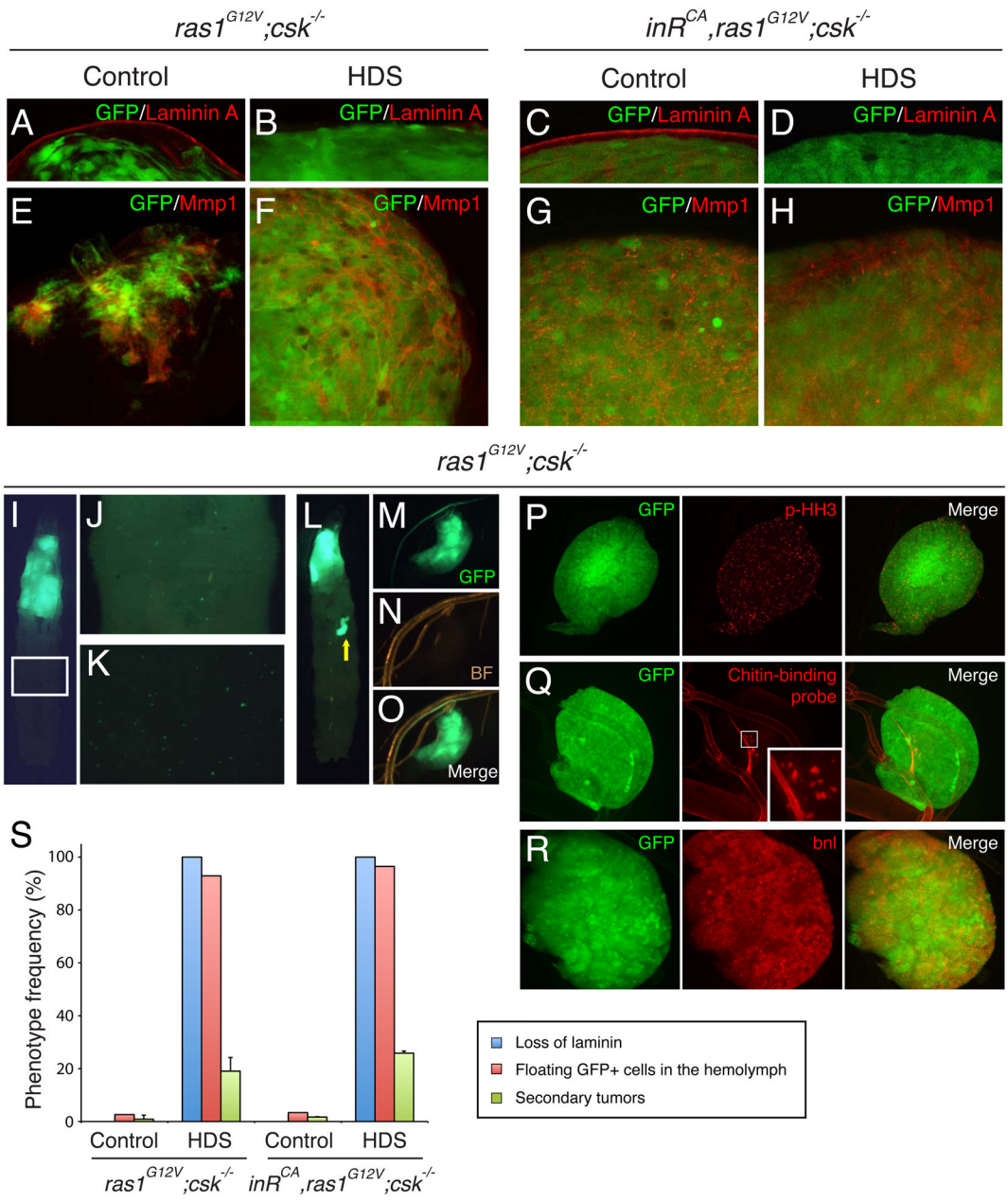

Figure 2. Ras/Src-tumors in HDS spread into hemolymph and colonized near trachea to form secondary tumors

(A–D) Laminin A staining (red) of developmental stage matched *ras1*^{G12V};*csk*$^{-/-}$ or *inR*^{CA},*ras1*^{G12V};*csk*$^{-/-}$ eye discs raised on indicated diets. (E–H) MMP1 staining (red) of developmental stage matched *ras1*^{G12V};*csk*$^{-/-}$ or *inR*^{CA},*ras1*^{G12V};*csk*$^{-/-}$ eye discs raised on indicated diets. (I–K) Ventral view of *ras1*^{G12V};*csk*$^{-/-}$ animals raised on HDS (I). Zoom up of the inset is shown in (J), and the extracted hemolymph on mineral oil is shown in (K). (L–O) *ras1*^{G12V};*csk*$^{-/-}$ animals raised on HDS with growing secondary tumor (arrow). GFP (M), bright field (BF)(N) and merged image (O) of the dissected secondary tumor is shown. (P) phospho-Histone H3 staining (p-HH3; red) of *ras1*^{G12V};*csk*$^{-/-}$ secondary tumor. (Q) Chitin-binding probe staining (red) of *ras1*^{G12V};*csk*$^{-/-}$ secondary tumor attached to trachea. Zoom up of the inset is shown in the middle panel. (R) Branchless staining (bnl; red) of a

ras1^{G12V}*;csk*$^{-/-}$ secondary tumor attached to trachea. (S) Phenotype quantitation. Blue bar: % animals with loss of Laminin staining in the eye discs. Red bar: % animals with GFP-positive cells in the hemolymph. Green bar: % animals with secondary tumors. Results are shown as mean ± SEM. See also Figure S2.

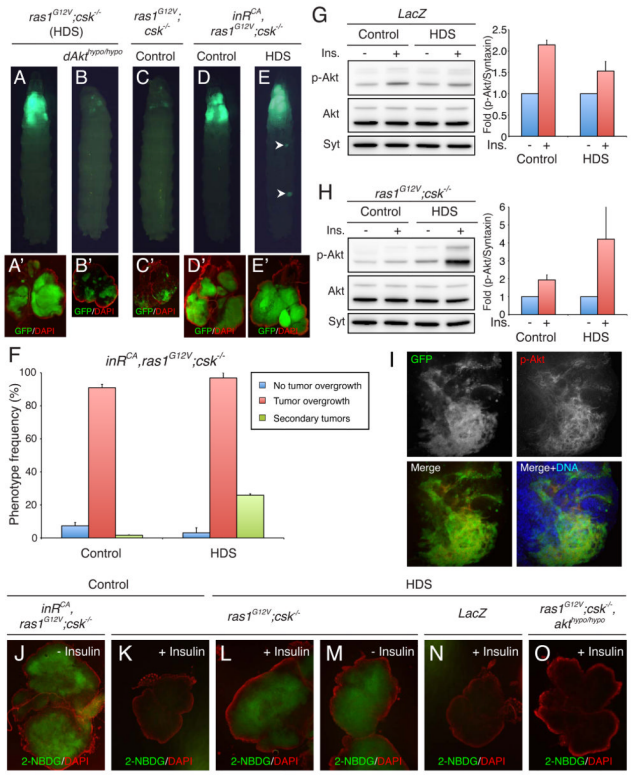

Figure 3. Ras/Src-activated cells evade insulin resistance

(A and B) Developmental stage matched animals raised on HDS with the genotype, (A) *ras1*^{G12V}*;csk*$^{-/-}$, (B) *ras1*^{G12V}*;csk*$^{-/-}$*,akt*$^{hypo/hypo}$, (C and D) Developmental stage matched animals raised on control diet with the genotype, (C) *ras1*^{G12V}*;csk*$^{-/-}$, (D) *inR*^{CA}*,ras1*^{G12V}*;csk*$^{-/-}$. Note that *inR*^{CA}*;ras1*^{G12V}*;csk*$^{-/-}$ animals fed control diet led to overgrowth but not secondary tumor formation. (E) *inR*^{CA}*,ras1*^{G12V}*;csk*$^{-/-}$ animals fed HDS. (A′–E′) Matching dissected eye epithelial tissue stained with DAPI (red). (F) Quantitation of the observed phenotypes. The three color bars are explained in the legend of Fig. 1J. Results are shown as mean ± SEM. (G and H) Dissected eye tissue of *lacZ* (G) or *ras1*^{G12V}*;csk*$^{-/-}$ (H) animals fed control diet or HDS were treated with or without Insulin, and total Akt, phospho-Akt (p-Akt), and Syntaxin (Syt) levels were examined by immunoblotting. The results of immunoblots were quantitated using Image J software and p-Akt/Syt values relative to subject without Insulin stimulation were determined. Results are shown as mean ± SEM. (I) Dissected eye tissue from *ras1*^{G12V}*;csk*$^{-/-}$ animals fed HDS were treated with Insulin, and immunostained with anti-phospho-Akt (p-Akt) antibody. (J–O) Glucose uptake was examined by uptake of 2-NBDG of the dissected eye tissue from *inR*^{CA}*,ras1*^{G12V}*;csk*$^{-/-}$ (J), *ras1*^{G12V}*;csk*$^{-/-}$ (K–M), *lacZ* (N), or *ras1*^{G12V}*;csk*$^{-/-}$*,akt*$^{hypo/hypo}$ (O) animals fed control diet or HDS, with or without Insulin stimulation. See also Figure S3.

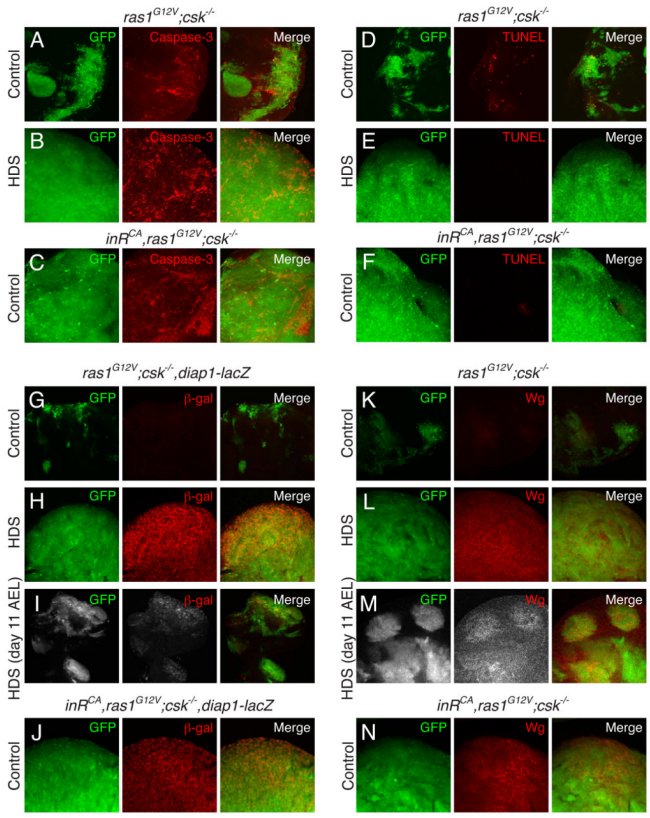

Figure 4. Ras/Src-tumors are resistant to apoptosis in high sucrose diet

(A–C) Cleaved Caspase-3 staining (red) of *ras1*^{G12V}*;csk*$^{-/-}$ (A and B) or *inR*^{CA}*,ras1*^{G12V}*;csk*$^{-/-}$ (C) eye discs raised on indicated diets. (D–F) TUNEL assay (red) was used to label apoptotic cell death of *ras1*^{G12V}*;csk*$^{-/-}$ (D and E) or *inR*^{CA}*,ras1*^{G12V}*;csk*$^{-/-}$ (F) eye discs raised on indicated diets. (G–J) β-galactosidase (β-gal) staining (red) of eye discs from *ras1*^{G12V}*;csk*$^{-/-}$*,diap1-lacZ* animals in a control diet (G), HDS at day 13 AEL (H), HDS at day 11 AEL (I), and *inR*^{CA}*,ras1*^{G12V}*;csk*$^{-/-}$*,diap1-lacZ* animals in a control diet (J). (K–N) Wingless (Wg) staining (red) of eye discs from *ras1*^{G12V}*;csk*$^{-/-}$ animals in a control diet (K), HDS at day 13 AEL (L) HDS at day 11 AEL (M), and *inR*^{CA}*,ras1*^{G12V}*;csk*$^{-/-}$*,diap1-lacZ* in a control diet (N). See also Figure S4.

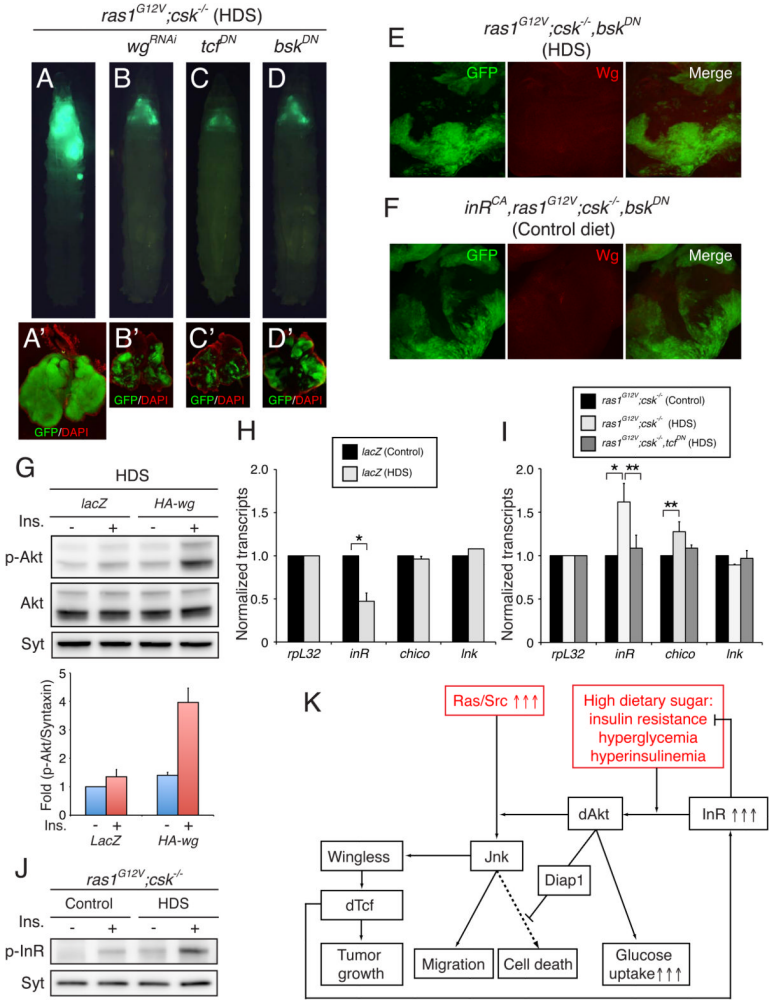

Figure 5. Wg mediates Ras/Src-tumorigenesis in HDS

(A–D) Animals raised on HDS with the genotype, (A) *ras1*^{G12V}*;csk*$^{-/-}$, (B) *ras1*^{G12V}*;csk*$^{-/-}$*wg,* ^{RNAi}, (C) *ras1*^{G12V}*;csk*$^{-/-}$*,tcf*^{DN}, (D) *ras1*^{G12V}*;csk*$^{-/-}$*,bsk*^{DN}. (A′–D′) Matching dissected eye epithelial tissue stained with DAPI (red). (E and F) Wingless (Wg) staining (red) of *ras1*^{G12V}*;csk*$^{-/-}$*,bsk*^{DN} eye discs raised on HDS (E) and *inR*^{CA}*,ras1*^{G12V}*;csk*$^{-/-}$*,bsk*^{DN} eye discs raised on a control diet (F). (G) Dissected eye tissue of LacZ control or HA-Wg animals fed HDS were treated with or without Insulin, and total Akt, phospho-Akt (p-Akt), and Syntaxin (Syt) levels were examined by immunoblotting. The results of immunoblots were quantitated using Image J software. Results are shown as mean ± SEM. (H and I) Histogram showing the levels of *rpL32*, *inR*, *chico*, and *lnk* mRNAs measured by quantitative RT-PCR. Total RNA was isolated from LacZ-expressing control eye discs (H) or *ras1*^{G12V}*;csk*$^{-/-}$ eye discs (I) raised on a control diet (Black bar) or HDS (White bar) or *ras1*^{G12V}*;csk*$^{-/-}$*,tcf*^{DN} eye discs raised on HDS (Grey bar). Results are shown as mean ± SEM. Asterisks indicate statistically significant difference (*, $p<0.01$; **, $p<0.05$). (J) Dissected eye tissue of *ras1*^{G12V}*;csk*$^{-/-}$ animals fed control diet or HDS were treated with or without Insulin, and phospho-Insulin Receptor (p-InR) and Syntaxin (Syt) levels were examined by immunoblotting. (K) Model of diet-mediated tumorigenesis of Ras/Src-activated cells. See also Figure S5.

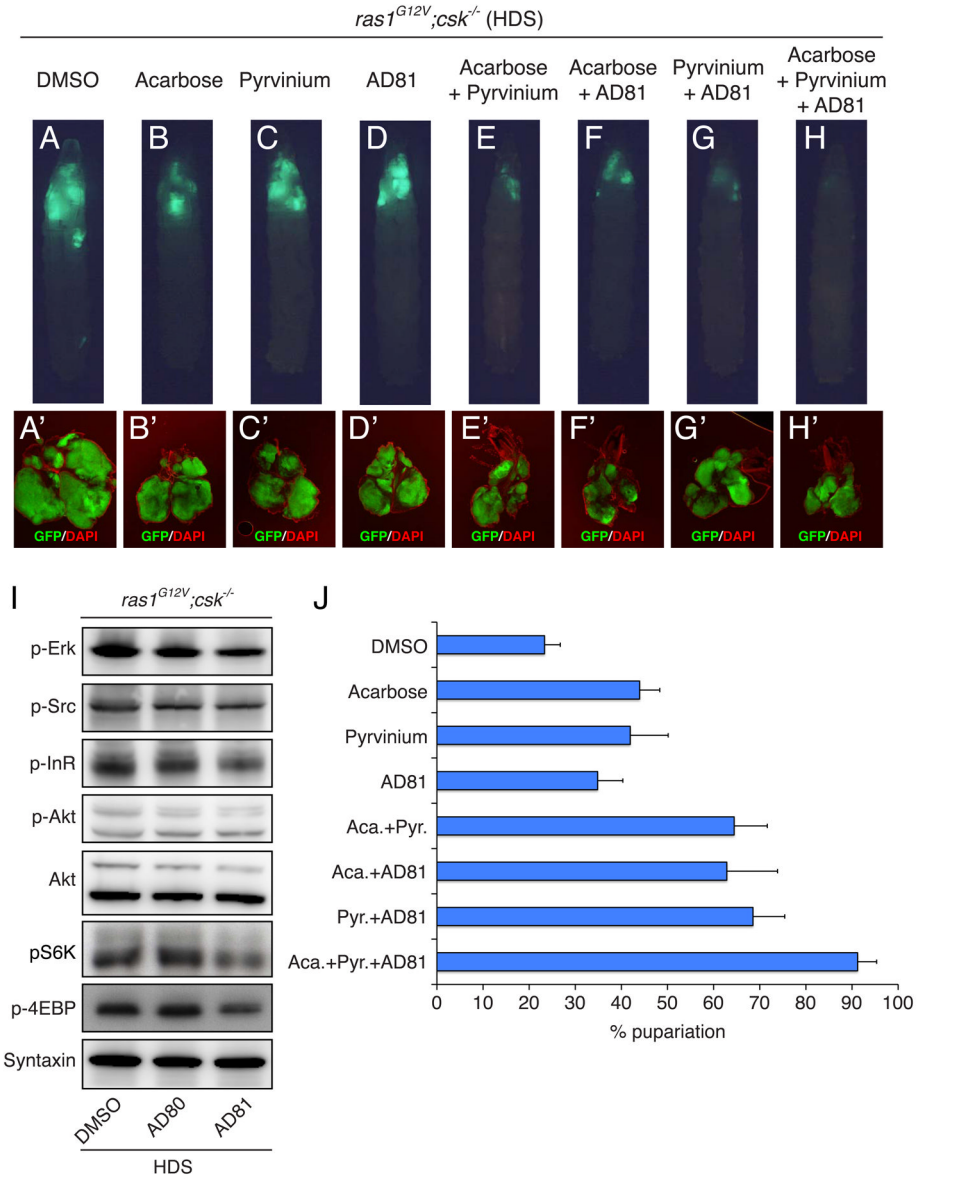

Figure 6. Combinatorial multi-node drug treatment for Ras/Src-tumors in HDS

(A–H) *ras1*^{G12V};*csk*$^{-/-}$ animals fed HDS containing (A) 0.05% DMSO, (B) 20 μM acarbose, (C) 25 μM pyrvinium, (D) 50 μM AD81, (E) 20 μM acarbose plus 25 μM pyrvinium, (F) 20 μM acarbose plus 50 μM AD81, (G) 25 μM pyrvinium plus 50 μM AD81, (H) 20 μM acarbose plus 25 μM pyrvinium plus 50 μM AD81. All phenotypes were assessed at day 17 AEL. (I) Cell extracts from dissected eye tissue of *ras1*^{G12V};*csk*$^{-/-}$ animals fed HDS supplemented with DMSO, AD80 or AD81 were examined by immunoblotting. (J) Percent pupariation of DMSO- or drug-treated *ras1*^{G12V};*csk*$^{-/-}$ animals was determined at day 17 AEL. Results are shown as mean ± SEM. See also Figure S6.